J. Ocean Univ. China (Oceanic and Coastal Sea Research)
https://doi.org/10.1007/s11802-023-5432-9
ISSN 1672-5182, 2023 22 (5): 1277-1288
http://www.ouc.edu.cn/xbywb/
E-mail:xbywb@ouc.edu.cn

Experimental Study of Submergence Ratio on Local Scour Around a Square Pile in Steady Flow

DU Shengtao[1)], WU Guoxiang[2), *], LIANG Bingchen[2), 3)], ZHU David Z.[1)], and WANG Risheng[4)]

1) *School of Civil and Environmental Engineering*, *Ningbo University*, *Ningbo* 315211, *China*
2) *College of Engineering*, *Ocean University of China*, *Qingdao* 266100, *China*
3) *Shandong Provincial Key Laboratory of Ocean Engineering*, *Ocean University of China*, *Qingdao* 266100, *China*
4) *College of Civil Engineering*, *Shandong Jiaotong University*, *Jinan* 250357, *China*

(Received May 22, 2022; revised August 16, 2022; accepted October 4, 2022)

Abstract Scour around a submerged square pile was realized experimentally in a steady flow to study the effects of flow depth on local scour. Flow depth to pile height ratios ranging from 1.5 to 5 in uniform sand and 2 to 5 in non-uniform sand were tested in the approaching flow velocity to critical velocity (larger than which the sediment particle is motivated) ratios of 0.56 and 1.03, respectively. The influences of flow depth were investigated on the basis of analysis of the three-dimensional topography, temporal maximum scour depth, bed profile development, and equilibrium scour depth. Results showed that the maximum scour depth was at the upstream corners of the pile other than at the stagnation point. The evolutions of the maximum scour depth data in non-uniform sand were well fitted with a recent exponential function, which characterized the initial, developing, and equilibrium stages of scour depth. The scour hole slopes upstream of the pile were found to be parallel to each other in the process of each test and were mainly governed by the sediment repose underwater. The equilibrium scour depth varied slightly with flow depth when the submergence ratio was larger than 1 in uniform sand while it was 2 in non-uniform sand. The armoring effects of coarse sediment particles markedly reduced the sediment transport in non-uniform sand despite the 0.34 increment in non-uniformity.

Key words non-uniform sand; square pile; local scour; submerged; scour depth

1 Introduction

Local scour around structures, such as bridge piers, pipelines, caissons, and breakwaters, are commonly found in fluvial or coastal engineering. In the US, Hunt (2009) investigated 1000 cases of bridge failures and found that over 50% were due to local scour, while Liu *et al*. (2017) noted approximately 40% in China. In addition to the wave-induced loads (Gao *et al*., 2020, 2021; Wang *et al*., 2022), structures in coastal engineering are also under the threat of local scour induced by waves or currents. An example of scour depth around a monopile near the Dutch coast with scouring waves and currents for a few months was found to be even larger than its diameter (Rudolph *et al*., 2008). Furthermore, a semi-submerged ship was broken off during its operation on a coast in Jiangsu, China, in May 2021. One of the main reasons for this breakage was local scour, which eroded the seabed under the ship. These effects of local scour deeply uncovered the structures and introduced additional bearing forces during exposure of the structure to flow, weakening the structure stability and leading to economic loss (Bordbar *et al*., 2021).

* Corresponding author. E-mail: guoxiang@ouc.edu.cn

Numerous researchers have studied the mechanism and scour depth of local scour around a single cylinder to predict the maximum scour depth and provide a comprehensive understanding of local scour protection. Flow accelerations or wake vortices control the local scour process in wave-only conditions (Sumer and Fredsøe, 2002), while horseshoe vortices and flow accelerations govern such a process under current-only conditions (Roulund *et al*., 2005; Zhao *et al*., 2012; Guan *et al*., 2019). Some latest studies can be found in Alejandra *et al*. (2021), Yang *et al*. (2021), OuYang *et al.* (2022), and Williams *et al.* (2022). The local scour around a structure (*e.g*., an infinite cylinder) involves remarkably complex flow-structure-sediment interactions. When a cylinder is settled in a sandy seabed, the flow in the vicinity of cylinder will be changed. The horseshoe vortex in front of the cylinder, flow acceleration at upstream cylinder corners, and vortex shedding behind the cylinder, will amplify the shear stress near the bed and thus induce sediment transport (Roulund *et al*., 2005). Researchers found that the maximum scour depth around a cylinder was dependent on the flow depth, flow velocity, sediment particle size, sediment non-uniformity, pile height, pile width, pile cross-section geometry, skew angle of the pile, and scour time (Melville and Chiew, 1999; Sumer and Fredsøe, 2002; Liang *et al*., 2020; Alejandra *et al*., 2021). In the works of

scour protections, bed armoring countermeasures and flow altering methods are the two major ideas used to reduce scour depth by riprap or stones and weaken the horseshoe vortex *via* collar base, sacrificial pile, and tetrahedral frame (Zhang *et al*., 2021).

The noted influential factors on local scour, especially effects on the maximum scour depth, have been extensively studied. Studies in predicting the equilibrium scour depth, that is, the asymptotical value of the maximum scour depth, were mainly focused on non-dimensional parameters through the Buckingham π-theorem analysis. According to the theorem and Simarro *et al.* (2007), the equilibrium scour depth of a cylinder can be written in a function as in Eq. (1):

$$\frac{d_{se}}{D}=f(\frac{\rho_s}{\rho},\sigma,\frac{h}{D},\frac{D}{d_{50}},\frac{gd_{50}^3}{\upsilon^2},\frac{U}{U_c}), \tag{1}$$

where d_{se} is equilibrium scour depth; D is pile width; ρ and ρ_s are water and sediment density, respectively; h is flow depth; υ is flow viscosity; d_{50} is median sediment diameter; σ is sediment non-uniformity; g is gravity acceleration; U is the depth-averaged velocity in approaching flow; U_c is the minimum velocity to motivate the sediment particle.

In non-uniform sand conditions, fine sediments were armored by the coarse sediment particles when scoured. Oliveto and Hager (2002) and Mir *et al.* (2018) found that scour rate and equilibrium scour depth dramatically decreased with the increasing value of non-uniformity. Melville and Chiew (1999) summarized the influences of relative flow depth (h/D) on local scour and classified it into the following three levels: the narrow pile of $h/D\geq1.4$, medium width pile of $0.2<h/D<1.4$, and wide pile of $h/D\leq0.2$. The relative equilibrium scour depth (d_{se}/D) is independent of h/D in the first level while d_{se}/D increased with the rising h/D in the third level. Sheppard *et al.* (2004) experimentally studied the factor of relative sediment size (D/d_{50}) through large-scale models and found that d_{se}/D was independent of D/d_{50} when the latter was approximately $25-50$.

However, reports on local scour around a submerged square pile, which can represent a series of underwater structures, such as subsea pipeline foundations, manifolds, and caissons (Zhao *et al*., 2012), are few. The authors believe that the related works can only be found in Zhao *et al.* (2012), Sarkar (2014), Yao *et al.* (2018), and Du and Liang (2019). The blunt nose of a square pile has been found to induce larger shear stress than a circular pile (Tseng *et al.*, 2000). Therefore, scour depths in square piles were substantially large (Khosronejad *et al*., 2012), especially in clear-water scour conditions. Empirical equations that are mainly based on the circular pile data usually multiply a large coefficient to predict the equilibrium scour depth of the square pile accurately (*e.g*., the local scour depth design method in Melville and Chiew (1999)). Du and Liang (2019) recently tested the local scour around circular and square piles with the same width and found that the equilibrium scour depth of the former was more than ten times of the latter.

In addition to the pile shape effect, flow depth is another important factor in local scour. Many studies in an infinite cylinder (*i.e*., unsubmerged pile, studies on the submerged pile are confined) are available. Flow structures in a submerged case are remarkably different from the unsubmerged case (Lacey and Rennie, 2012). The flow pattern significantly varies when the pile height to pile width ratio (h/D) is between 2 to 4, while vortex shedding changes from the Karman type to the arch type (Okamoto and Sunabashiri, 1992). In addition, the interactions between the bow wave and the horseshoe vortex upstream at the pile face would diminish the strength of the vortex in an unsubmerged pile, while the upward flow will pass by the top of the pile in a submerged case (Dey *et al*., 2008). Furthermore, the downwash due to reverse flow at the pile top produces reverse pressure at the pile tail (Tsutsui, 2012). These different turbulences were found to have important effects on local scour (Dey *et al*., 2008; Yao *et al*., 2018).

Studies regarding local scour around the submerged piles (circular and square) in steady current are few. Shamloo *et al.* (2001) studied the flow structures and characteristics of local scour around a submerged hemisphere shape obstacle whose flow depth to its height (h/l) ranged from $0.62-4.27$ in clear-water scour conditions and observed four regimes of flow pattern that were related to quite different four scour patterns. Dey *et al.* (2008) investigated the submerged circular piles in clear-water scour conditions and proposed a coefficient representing the ratio of the equilibrium scour depth of a submerged cylinder to that of an unsubmerged cylinder with the same diameter. Zhao *et al.* (2010) found that equilibrium scour depth was almost independent of the pile height-to-width ratio (l/D) when the latter was larger than 2 in live-bed scour conditions. When the ratio was smaller than 2, the near-bed shear stress of the high pile had a large and wide horseshoe vortex, thus inducing deep scour holes. Euler and Herget (2011) replaced the pile width with an equipment length and added the Froude number as a second dimensional parameter in a developed model, which was a Reynolds number-based approach to estimate the maximum scour depth of submerged cylinders. Zhao *et al.* (2012) examined the rectangular and square piles with $l/D\leq1$ in live-bed scour conditions, in which the equilibrium scour depth increased with the pile height. Sarkar (2014) experimented with a series of submerged circular and square piles under clear-water scour conditions sand and obtained two fitted equations that were used to estimate the equilibrium scour depths of the circular and square piles, respectively. Yao *et al.* (2018) designed a wide range of local scour tests around the submerged circular and square piles from nearly live-bed scour to sheet flow. They found that the equilibrium scour depth decreased with the increasing l/D and was independent of l/D when l/D was smaller and larger than 4, respectively. The above reviews in literature attempted to study the flow depth to pile width ratio effects on local scour.

Nevertheless, each study of the submerged case was experimented with in its constant flow depth that cannot reflect the real influences of flow depth on local scour in submerged conditions. This paper aims to investigate the

effects of flow depth and sediment non-uniformity on the local scour around a submerged square pile, emphasizing the variations of the maximum and equilibrium scour depths of a submerged square pile. The remaining sections are organized as follows. First, the experimental test processes, including the velocity and bed profile measurements, are introduced. The results of local scour in uniform sand with a medium size of 0.65 mm are then presented and discussed. Afterward, the differences between uniform and non-uniform sand with a medium size of 0.18 mm and a high velocity are compared. Finally, conclusions are provided.

2 Experimental Setup

Experimental tests were conducted in a 60 m long, 1.2 m wide, and 1.5 m deep flume in the Hydraulic Modeling Laboratory at Shandong Jiaotong University, China. As shown in Fig.1, water was pumped from the inlet to the outlet and was recirculated by a pipe outside. A 10 cm × 10 cm × 30 cm sized square pile model comprising acrylic block materials was embedded in the 20 cm height sand bed. The embedded model was 32.4 m downstream of the inlet, which ensured the complete development of the approaching flow. The sand bed was 8.4 m long, 1.2 m wide, and 0.2 m high, with a slope of 1:6 at each side.

Uniform and non-uniform sand were used in the experiments. Their medium grain sizes were 0.65 and 0.18 mm, and the sediment non-uniformity $\sigma=(d_{85}/d_{15})^{0.5}$ was 1.27 and 1.6, respectively. Calculated by the equation of $\tan(\alpha_d)=0.74d_{50}^{0.05}$ (Cheng and Zhao, 2017), their angles of static repose (α_d) underwater were 36.5° and 36.3°. Each of the specific gravity of sediment grain density was 2.65. Each of the medium sediment sizes was between 0.1 and 1 mm. Thus, the critical shear velocity (u_{c*}) for sediment was determined from $u_{c*}=0.0115+0.0125d_{50}^{1.4}$, which approximated the Shields diagram (Melville, 1997). The critical average velocity (U_c) was calculated from

$$\frac{U_c}{u_{c*}}=5.75\log(5.53\frac{h}{d_{50}}).$$

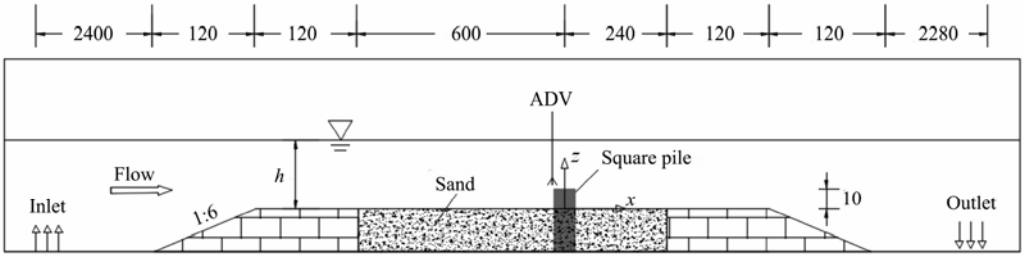

Fig.1 Test flume and coordinate system establishment (unit: cm).

However, the fine sediment particles for nonuniform sand are armored by the coarse particle when scoured (Melville and Sutherland, 1988). The flow intensity is calculated by $\frac{U-(0.8U_{ca}-U_c)}{U_c}$, wherein U_{ca} is the depth-averaged flow velocity beyond which armoring effects do not occur in a non-uniform sand bed. The U_{ca} is also determined from the above equations in Melville (1997), with $d_{50a}=\sigma^m d_{\max}/1.8=\sigma^m d_{50}/1.8$ being the coarsest possible armor, $m=$ 1.28, 1.65, 2.06, and 2.34 when the maximum sediment particle sizes are d_{90}, d_{95}, d_{98} and d_{99}, respectively. The averaged flow intensity of $\frac{U-(0.8U_{ca}-U_c)}{U_c}$ was calculated at 1.03, which was slightly larger than the limit value of the clear-water scour condition.

The approaching velocity was measured at the position where the pile model would be settled by a Nortek Vectrino II Acoustic Doppler Velocimeter (ADV), whose probe can measure velocities with an accuracy of ±0.1 mm s^{-1}. The designed depth-averaged velocities were obtained from the flow rate, which was controlled by the water pump system. Table 1 shows that water depths ranging from 15 to 50 cm in tests A1–A5 were maintained with approaching velocity to the critical velocity ratio (U/U_c) (*i.e.*, flow intensity (Guan *et al.*, 2019)) of 0.55–0.56 while they were 20 to 50 cm in tests B1–B4 with a constant value of 1.03. Test C was experimented with in a water depth of 30 cm with a depth-averaged velocity of 24.4 cm s^{-1}, which was the same as test B2. The scour time needed for the equilibrium scour depth increased with the rising flow intensity. Thus, the duration of experiments (t_d) in tests A1–A5 was kept at 1080 min while that in B1–B4 was substantially long. In the process of local scour tests, temporal scour depths of $d_s(t)$ and $d_c(t)$ at upstream pile corners ($x/D=-0.5$, $y/D=\pm0.5$) and stagnation point ($x/D=-0.5$, $y=0$), respectively, where the maximum scour depth was expected, were observed through the distance function of ADV (accuracy of ± 1 mm) and the bed profile elevations. The water was drained slowly after the pump was stopped at the end of each test. The final scour depths at upstream pile corners (d_s) and stagnation point (d_c) were checked by the tick marks pasted on the pile model.

3 Scour in Uniform Sand

3.1 Bed Topography Around the Pile

Bed topography around the pile was measured at the end of the scour test to investigate the effect of flow depth on sediment scour and deposition around the square pile. In the entire process of each test, no sediment transport was observed in approaching flow, indicating that local

scour tests of A1 – A5 were in clear-water scour conditions. The flow intensity was approximately 0.56 for each test. As presented in Figs.2a – d, sediment scour and deposition were similar in all the tests. For each test, a scour hole was formed upstream of the pile, and sand dunes were distributed on both sides of the pile. Notably, the result of test A3 was almost the same as test A2. Therefore, this result was not presented herein. The maximum scour depth was at the upstream corners of the pile and ranged from 0.2D to 0.24D in tests A1 – A5, as listed in Table 1. Additional details of the maximum scour depth can be found in Section 3.2.

Table 1 Parameters of the experimental tests

Test	d_{50} (mm)	σ	l (cm)	S	U (cm s^{-1})	U/U_c	t_d (min)	d_s (cm)	d_c (cm)
A1	0.65	1.27	10	0.5	18.2	0.56	1080	2.0	0
A2	0.65	1.27	10	1.0	18.9	0.55	1080	2.2	0
A3	0.65	1.27	10	2.0	20.0	0.56	1080	2.2	0
A4	0.65	1.27	10	3.0	20.7	0.56	1080	2.1	0
A5	0.65	1.27	10	4.0	21.6	0.56	1080	2.4	0.3
B1	0.18	1.60	10	0.5	23.3	1.03	480	4.2	2.2
B2	0.18	1.60	10	2.0	24.4	1.03	840	4.8	2.5
B3	0.18	1.60	10	3.0	25.2	1.03	480	4.7	2.1
B4	0.18	1.60	10	4.0	25.8	1.03	840	5.0	3.5

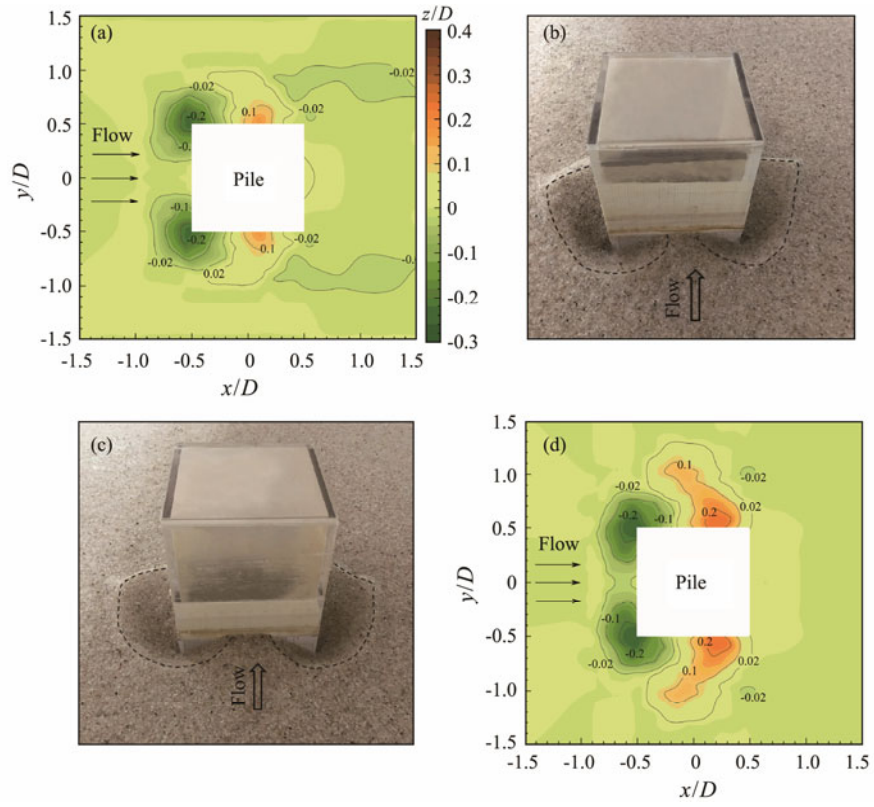

Fig.2 Topography and pictures of the tests at t_d = 1080 min. (a), test A1; (b), test A2; (c), test A4; (d), test A5.

The scour hole diameters of tests A1 and A5 were approximately 0.35D and 0.36D, respectively. Scour holes extended from upstream corners toward the stagnation point. However, the boundaries of scour holes along the x/D = −0.5 profile ranged from −0.4D to −0.35D in tests A1 – A4. Owing to the large scour hole size, sand dunes in test A5 were 0.1D higher and 0.3D more extensive than in test A1 in the y-direction. Minimal sediment scour or deposition was observed behind the pile. Except for the 0.03D scour depth of test A5 (Fig.2d), minimal or no scour was either observed at the stagnation point (Figs.2a, b, and c). These phenomena were remarkably different from local scour around a circular pile whose maximum scour depth was usually at the stagnation point in clear-water scour conditions (Dey *et al*., 2008).

In local scour around a square pile, the combinations of flow accelerations and horseshoe vortex at pile upstream corners contributed to the scour (Zhao *et al*., 2012). Local scour was induced by the amplified shear stress near the bed (Roulund *et al*., 2005). Thus, the initiation of scour at the upstream corners and the far lower scour depth at the stagnation point indicated that the horseshoe vortex upstream played a slightly important role while the flow accelerations were dominant in local scour. When flow depth surpassed 4D, the horseshoe vortex, which was induced by the down flow, boundary layer separation near the bed,

and reverse pressure at the pile face (Sumer and Fredsøe, 2002), was sufficiently strong to roll up sediment particles at stagnation point and its vicinity. Despite the 0.03D scour depth at the stagnation point, and 0.1D high hills in test A5, the scour and deposition characteristics in Fig.2 illustrated that flow depth affected local scour minimally when $h/D \leq 5.0$.

3.2 Temporal Bed Profile and Maximum Scour Depth

Fig.3 presents the bed elevations along profile I–I' ($y/D = -0.53$) at various scour durations. The figures reveal that a scour hole and a sand dune around the pile emerged as scouring progressed in each test. The temporal bed profiles showed minimal change in the scour holes or sand dunes after 60 min scouring, indicating that local scour attained an equilibrium state. This phenomenon is consistent with the temporal scour depth at upstream corners in Fig.4, which shows that scour depth increased linearly in the first 60 min and maintained a constant value after that time. As shown in Fig.3, the maximum scour depth occurred at −0.5 D to −0.55D, with its value ranging from 0.18D to 0.21D. The scour hole slope upstream of the pile was 35.3°−37.5°, which was slightly smaller or larger than the slope angle of 36.5° under water. When the sediment was scoured by the horseshoe vortex upstream of the pile, the formation of a scour hole with a steep slope was observed in the scouring test. However, the sediment particles on the steep slope collapsed and fell into the scour hole with the increase in scour hole depth, resulting in a gentle slope (that is, the scour hole slope upstream of the pile in Fig.3). There

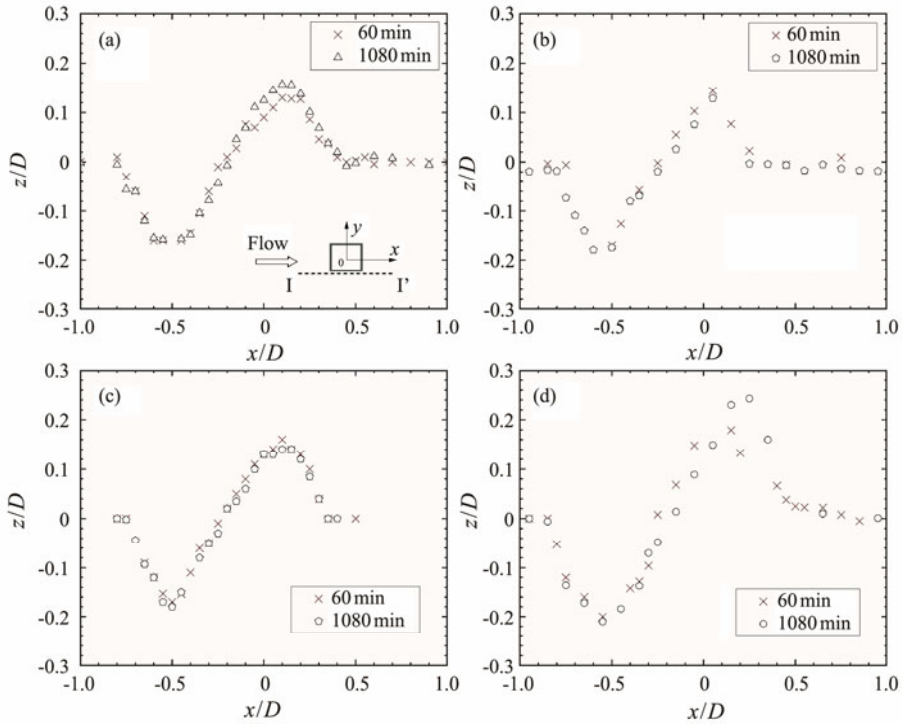

Fig.3 Bed elevations along profile I–I' ($y/D = -0.53$). (a), test A1; (b), test A2; (c), test A3; (d), test A5.

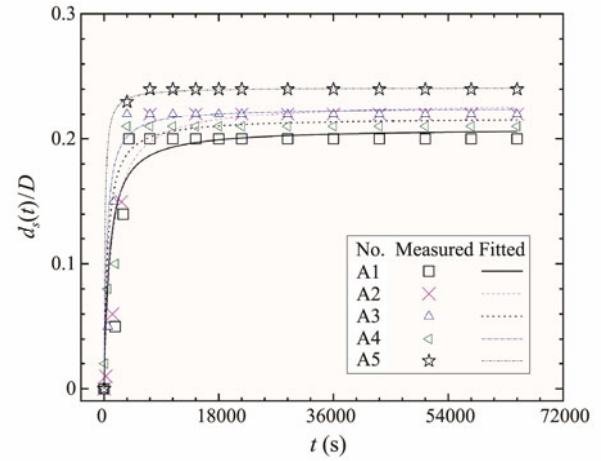

Fig.4 Temporal maximum scour depth of tests A1–A5 fitted with Eq. (2).

phenomena indicate that the size of scour hole was controlled by the combinations of horseshoe vortex and angle of sand static repose under water. The sediment par ticles in scour hole were then transported by flow and deposited in areas of −0.2D to −0.55D. The deposited sand dune was not eroded because of the weak wake vortex, ac- cording to Sumer and Fredsøe (2002), who stated that the wake vortex absorbed sediment particles that were behind the pile and transported them downstream. The height of the sand dune was approximately 0.18D at scour durations of 60 and 1080 min in tests A1–A3 (Figs.3a, b, and c) and increased from 0.19D to 2.3D in test A5 (Fig.3d) due to the large scour depth and size.

Temporal scour depth at upstream corners is shown in Fig.4 to investigate the maximum scour depth variations with scour durations. As expected, for each test, the scour depth increased rapidly in the first 60 min before it reached a maximum value, that is, the equilibrium scour depth. This

finding is consistent with Hong *et al.* (2012), who stated that the scour rate increased sharply with scour time in the initial stage, and the scour depth remained constant in the equilibrium stage. Briaud *et al.* (1999) and Sumer and Fredsøe (2002) proposed a hyperbolic function (2) and an exponential function (3), respectively, to predict the temporal maximum scour depth of an unsubmerged circular pile. Zhao *et al.* (2012) and Yao *et al.* (2018) found that the aforementioned functions were applicable in submerged square piles despite the maximum scour depth at upstream corners other than at the stagnation point in their results.

$$d_c(t) = d_{ce}[t/(t+T_0)], \tag{2}$$

$$d_c(t) = d_{ce}[1-\exp(-t/T_0)], \tag{3}$$

where $d_c(t)$ and d_{ce} are the scour depth and the equilibrium scour depth at the stagnation point of the pile, respectively, and T_0 is a constant that defines the time scale of the scour process.

The temporal maximum scour depth data and fitted curves based on Eq. (2) with the nonlinear least square method are shown in Fig.4, in which all the curves fit the data well. In addition, the minimum square of correlation coefficients calculated from Eqs. (2) and (3) was 0.9995 and 0.99996, respectively. The fitted curves of Eq. (3) were not presented herein for brevity. The curves in Fig.4 depict that scour depth at upstream corners reached the equilibrium scour depth in 120 min in each test. The local scour tests by Zhao *et al.* (2012) and Yao *et al.* (2018) were in live-bed scour conditions. Thus, the well fitted curves in Fig.4 illustrate that hyperbolic function (2) and exponential function (3) can be used to predict the temporal maximum scour depth around a submerged square pile in clear-water scour conditions. The laws of equilibrium scour depth with flow depth variations were discussed in Section 4.2 to realize a comparative comprehension of the flow intensity and sand non-uniformity of the flow depth effects.

4 Scour in Non-Uniform Sand

4.1 Topography and Bed Profiles

Tests B1−B4 were implemented to investigate the flow depth effects on local scour in non-uniform sand. Each test was conducted in a constant flow intensity of 1.03, as listed in Table 1. The final bed topography is presented in Fig.5. Overall, the scour holes and sand dunes were mainly upstream and behind the pile, respectively. The scour depth at the stagnation point was smaller than that at upstream corners for tests B1−B4 (Figs.5a−d), which was similar to the cases in tests A1−A5. This phenomenon also appeared in live-bed conditions in Zhao *et al.* (2012) and was attributed to the shortage of the pile and the insufficient flow intensity, which would result in a weak horseshoe vortex. Therefore, this phenomenon was probably due to the insufficiently strong horseshoe vortex upstream of the pile and the dominant flow accelerations at the pile upstream corners in the scour process. Yao *et al.* (2018) found that the maximum scour depth was at the stagnation point in the tests of local scour around submerged square piles, in which the flow intensity was 1.55, and the pile heights were 5.5 and 11 cm. Fig.5 reveals that the shapes of scour holes

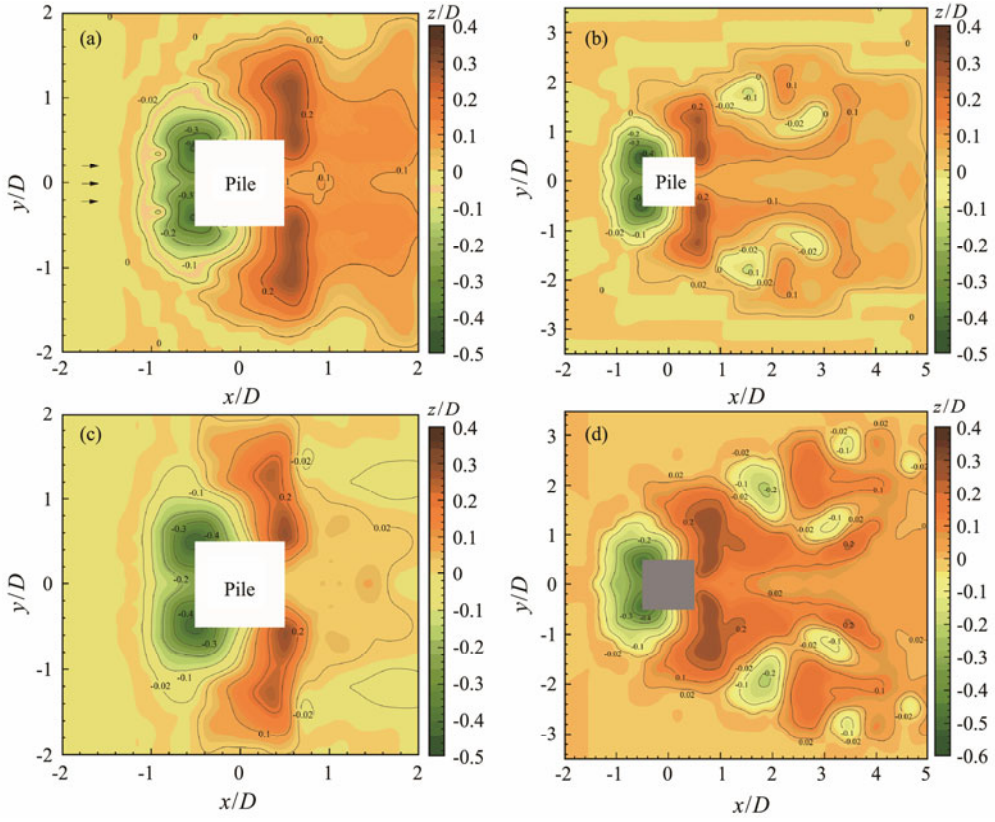

Fig.5 Final bed topography around the pile. (a), test B1, t_d=480 min; (b), test B2, t_d=840 min; (c), test B3, t_d=480 min; (d), test B4, t_d=840 min.

and sand dunes are remarkably similar to each other; that is, there are scour holes around the pile and two sand hills near or behind the lee side of the pile. Notably, scour duration in tests B2 and B4 was 840 min, while that in tests B1 and B3 was 480 min. The sizes of scour holes varied minimally with the increasing flow depth because the extents of scour holes ranged from 2.5D to 3.0D and 1.2D to 1.4D in transversal and longitudinal directions, respectively. Furthermore, the height and extent of sand hills in the longitudinal direction behind the pile were approximately 0.2D and 1.7D, respectively, in each test, indicating that the sediment transport forced by horseshoe vortex and flow accelerations upstream of the pile was in a similar grade because the sand dunes were related to the upstream horseshoe vortex and flow accelerations (Shamloo *et al*., 2001; Zhao *et al*., 2012).

The sediment depositions shown in Figs.5b and d were more extensive than those in Figs.5a and c due to the long scour duration. In addition to the thick sediment deposition downstream of the pile, secondary scour holes, and sand dunes appeared at the region of $1<x/D\leq4$ in tests B2 and B4, as respectively shown in Figs.5b and d. Five reasons were considered to be responsible for these phenomena. First, the turbulence energy was dismissed in the process of transporting sediment particles from the upstream scour hole, resulting in sedimentation downstream of the scour hole. Second, the sand dunes must adapt to match the angle of sediment repose to realize a stable state. Third, once the sand dunes close to the pile formed, a new horseshoe vortex would emerge behind the sand dunes, which would induce a new local scour, resulting in a secondary scour hole. Moreover, the size and extent of the secondary scour hole were limited because the strength of the new horseshoe vortex was weaker than the upstream horseshoe vortex. Last, the sediment transport rate induced by the wake vortex behind the pile was far less than the upstream horseshoe vortex; thus, the majority of sediment particles were deposited behind the pile. As the upstream boundary of scour hole was at approximately $x/D=-1.5$ and the sediment deposition extended more than 5D and 6D in transversal and longitudinal directions, respectively, a diameter of 1.5D scour protection region and more than 6.5D influencing region should be considered in a design project.

Figs.6a–d present the bed elevations along profile I–I' of tests B1–B4 at various scour durations. The shapes and patterns of the bed profiles in each test were similar; that is, scour and deposition were around the pile and behind the pile, respectively. The scour depth and sediment deposition height dramatically changed in the first 10 min, and the change slowed down gradually after this initial scour stage. During the local scour tests, sediment particles were scoured considerably rapidly by the flow accelerations at upstream corners, thus creating an initial scour hole. With ongoing scouring, the horseshoe vortex was later involved because of its remarkably complex and long forming process duration. The sediment particles collapsed and fell from the slope to maintain slope stability once an initial scour hole was scoured. The sediment particles in the bottom of scour hole were then raised and climbed along the opposite slope through the horseshoe vortex. The sediment particles in scour hole and slope repeated these processes until the strength of flow turbulence induced by flow accelerations and horseshoe vortex scour hole no longer had the capability to erode the scour hole deeply. The maximum scour depth was at approximately $x/D=-0.5$ in each test. With increasing flow depth, the maximum scour depth at the end of each test slightly increased, ranging from approximately 0.37D to 0.5D. The sand dunes behind the pile moved to the downstream direction slowly with increasing scour duration. However, the height of sand dunes is a constant value in each test (*e.g.*, 0.4D in test B3, Fig.6c), which indicated that the volume of sand transported from the scour hole and the sediment transport rate varied minimally in the four tests. The profiles that represented the slope of scour hole were almost parallel to each other at different scour durations at the region of $-1.5\leq x/D\leq0.5$ in each test. As mentioned in Section 3.1, the angle of sediment repose that

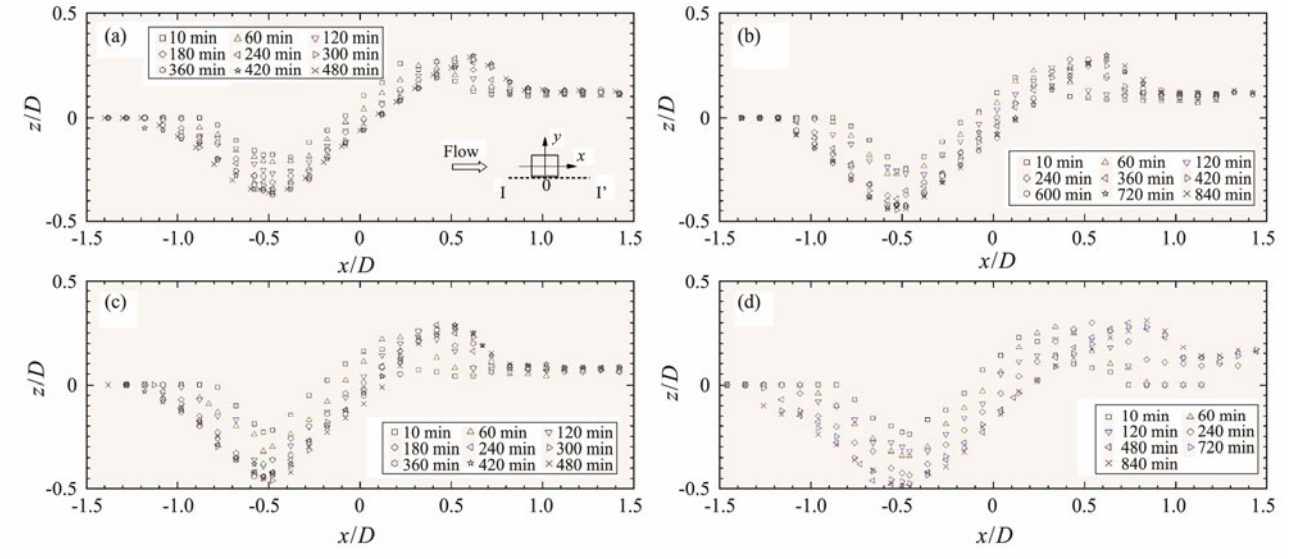

Fig.6 Temporal bed elevations along profile I–I' ($y/D=-0.53$). (a), test B1; (b) test B2; (c) test B3; (d), test B4.

controlled the slope and the flow turbulence, which was related to sediment transport from the scour hole, was attributed to these paralleled slopes.

4.2 Temporal Maximum and Equilibrium Scour Depth

The evolutions of the maximum scour depth of local scour undergo initial, developing, and equilibrium stages. With these concepts, Du and Liang (2019) advanced an exponential equation in Sheppard *et al.* (2004), which was found to be a well fitted function in estimating the maximum scour depth, as shown in Eq. (4). With $d_s(t)$ being the maximum scour depth at upstream corners at scour duration t; d_1 and d_2 are the scour depths in the initial and developing stages, respectively; T_1 and T_2 are the initial scour time scales of the initial and developing stages, respectively. In addition, Sheppard *et al.* (2004) and Du *et al.* (2022) found that the temporal maximum scour depth was substantially better fitted with Eq. (4) than Eq. (3) when the flow intensity was larger than 0.67.

$$d_s(t) = d_1\left[1-\exp(-\frac{t}{T_1})\right] + d_2\left[1-\exp(-\frac{t}{T_2})\right]. \quad (4)$$

Therefore, the time history data of the maximum scour depth of tests B1−B4 were curve fitted with Eqs. (2)−(4), as shown in Figs.7a−d. The equilibrium scour depths estimated by Eqs. (2) and (3) were smaller than Eq. (4), especially in tests B1 (Fig.7a) and B4 (Fig.7d). Furthermore, the minimum square of correlation coefficient (R^2) of the fitted curves using Eq. (4) was 0.985, while that using Eqs. (2) and (3) were 0.888 and 0.825, respectively, as shown in Fig.8. These results are probably attributed to the laws of sediment transport in the process of a local scour. In the initial stage, the sediment particles were transported rapidly in the scour hole, resulting in a sharp increase in the maximum scour depth. With the increase in scour hole, sediment particles that were transported from the scour hole comprised those particles that collapsed from the slope and deep erosion at the bottom of the scour hole; thus, the evolution of the maximum scour depth reached the developing stage. The duration of the developing stage of the maximum scour depth was substantially long because the scour hole around the pile in strong flow intensity conditions was substantially larger than that in weak flow intensity conditions.

The equilibrium scour depths of tests A1−A5 and B1−B4 were obtained from the measured data and fitted curves, respectively, by using Eq. (4) in Fig.7. Relationships of the relative equilibrium scour depth (d_{se}/D) with submergence ratio ($S=(h-l)/l$) and relative flow depth (h/D) were presented in Fig.9 to study the flow depth effects on the equilibrium scour depth. d_{se}/D increased with the rising h/D when $h/D<1.5$ for tests A1–A5. When $h/D\geq1.5$, d_{se}/D only slightly varied and tended to be a constant value of 0.22. This critical value of $h/D=1.5$ (larger than which d_{se}/D was independent of such a value) nearly equal to that was in the unsubmerged cases in Melville and Chiew (1999), who found values of 1.4 and 1.45, respectively. In the non-uniform sand tests of B1−B4, the fitted curve was remarkably similar to that in tests A1−A5. The relative equilibrium scour depth varied minimally from 0.45 to 0.51 for testes B1−B4. The d_{se}/D is independent of h/D when the latter was larger than 3. These findings were in accordance with Ettema *et al.* (2017), who stated that the adverse

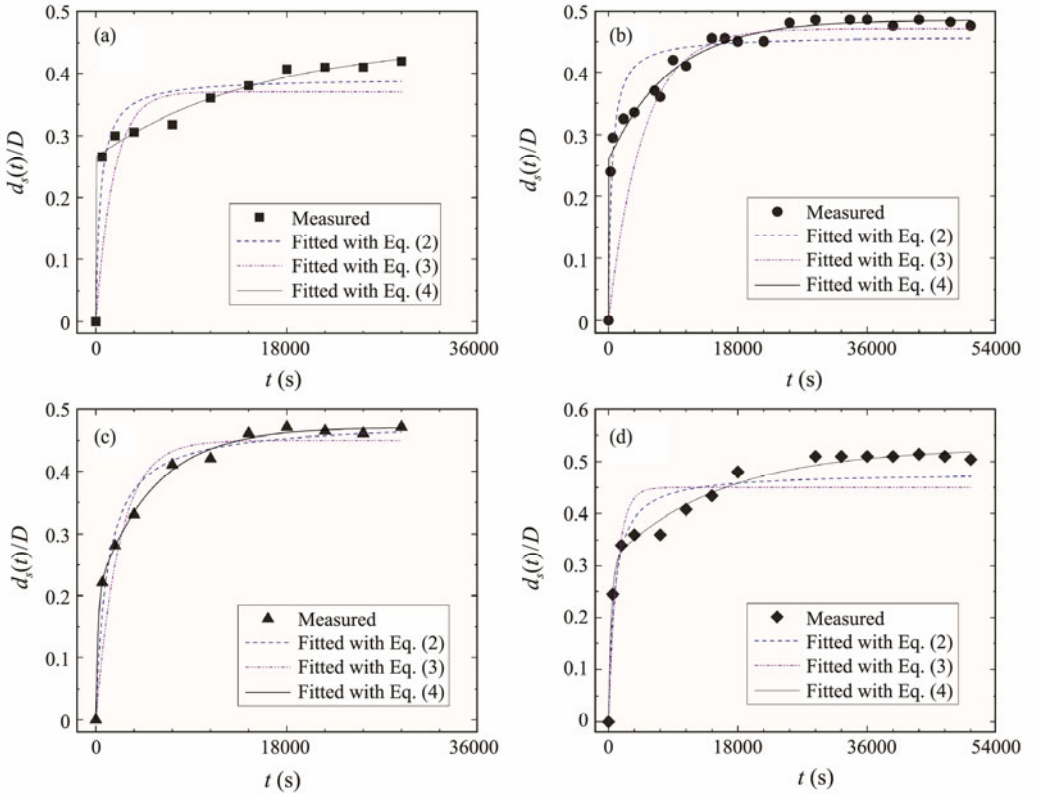

Fig.7 Temporal maximum scour depth of tests B1−B4 fitted with Eqs. (2), (3), and (4).

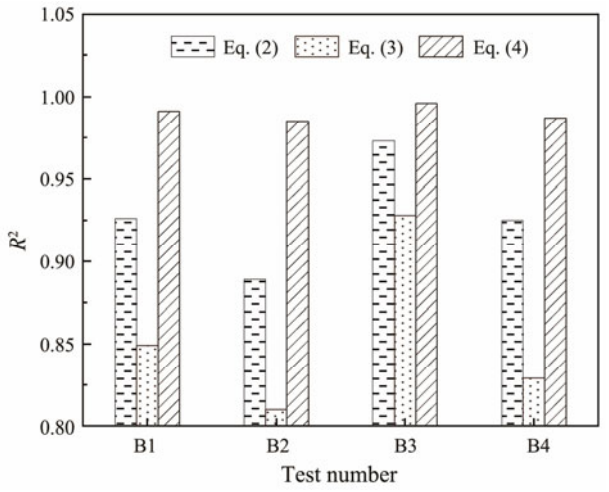

Fig.8 Square of correlation coefficients of equations fitted with measured data.

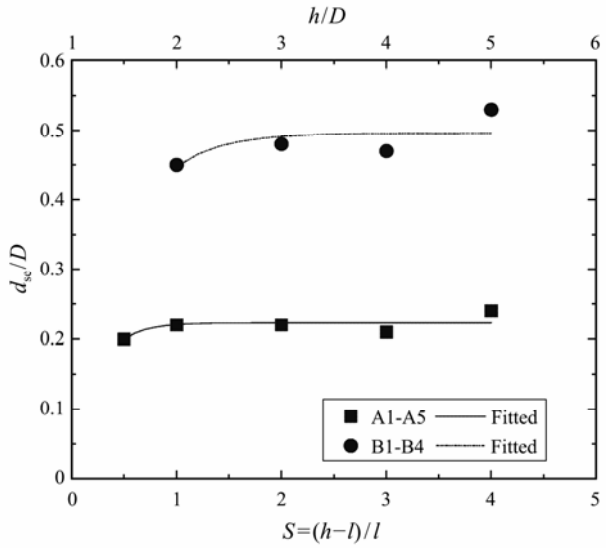

Fig.9 Relationships of submergence ratio with the relative equilibrium scour depth.

flow ahead of the pile would not interact with the horseshoe vortex when $h/D \leq 3$; thus, the strength of the horseshoe vortex would not be weakened by the adverse flow. However, by collecting a series of experimental data in the literature, Liang *et al.* (2020) found that the aforementioned strength was 4 in clear-water scour conditions through an envelope curve. The critical values of h/D obtained by different researchers varied in a range of 1.4 to 4 because the strengths of the horseshoe vortex and the flow accelerations corresponding to the maximum scour depth at upstream corners of the pile are also governed by flow intensity, pile geometry, and sediment non-uniformity. The trend lines of d_{se}/D and $S=(h-l)/l$ were remarkably similar to those of d_{se}/D and h/D. Fig.9 shows that the critical values of S, larger than which d_{se}/D were constant, were 1 and 2 in tests A1–A5 and B1–B4, respectively. These results indicated the downwash and reverse flow that described in Tsutsui (2012) would not affect the horseshoe vortex or the flow accelerations around the pile because the equilibrium scour depth was controlled by the horseshoe vortex and flow accelerations in local scour around a square pile in clear-water scour conditions. However, the critical value in tests B1–B4 ($\frac{U-(0.8U_{ca}-U_c)}{U_c}=1.03$) was slightly larger than that in tests A1–A5 (U/U_c), illustrating that this value was also affected by flow intensity.

5 Comprehensive Comparisons of Local Scour in Uniform and Non-Uniform Sand

A test C with $\sigma=1.26$ was also experimented to study the effects of sand non-uniformity on local scour. Except for the non-uniformity, test C was in the same experimental conditions as test B2; thus, the effects of sand non-uniformity on local scour could be analyzed by comparing the two tests. As shown in Fig.10 (test C), the scour hole around the pile had extended to the lee side of the pile. The relative length and width of the scour hole were approximately 2.3D and 3.4D, respectively, while those in test B2 were approximately 1.3D and 2.6D, respectively (Fig.5b). Nevertheless, the sand dunes behind the pile in test B2 were slightly high and extensive. The relative maximum scour depth and scour hole size in test C were substantially larger than those in test B2 despite the more than one time longer scour duration of the latter than the former. These findings were consistent with Melville and Chiew (1999), who found that the equilibrium scour depth decreased with the increasing sand non-uniformity due to the armoring effects provided by the coarse particles.

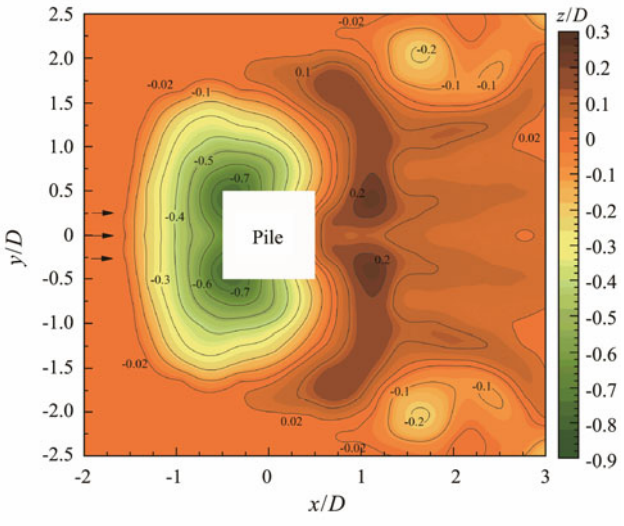

Fig.10 Final bed topography of test C.

Fig.11 depicts the temporal bed profiles of test C and the bed profile of test B2 at $t_d=360$ min. The bed profile evolutions of test C varied in similarity with those non-uniform sand tests in Figs.6a–d; that is, the profile is a stable stage asymptotically after intense sediment scour in the first 10 min. However, the profile of test B2 at $t_d=360$ min (the red cross-shaped symbols in Fig.11) was substan-

tially higher than test C (blue stars in Fig.11) at the same scour duration. In addition to the small scour depth, the bed profile that was related to the size of scour hole of test B2 was less extensive than test C. No sediment particles were replenished from the approaching bed when the flow intensity was no more than 1 in uniform sand. However, for non-uniform sand bed conditions, despite the scouring of some fine sediment particles approaching the bed and their transport into the scour hole around the pile, the fine sediment particles are armored by the coarse particles, resulting in a deduced sediment transport rate. The maximum scour depth of tests B2 and C in Fig.11, and the evolutions of the maximum scour depth at upstream corners of the two tests in Fig.12 illustrated that the sand nonuniformity led to a substantially small scour depth. The armoring effects of these coarse sediment particles affected the local scour in two ways: the coarsen bed form corresponding to a rough bed surface led to the weakened horse-shoe vortex, and the armoring effects in the scour hole resulted in less volume of sediment transport (Baker, 1979). These results were different from those in Melville and Chiew (1999), who stated that the armor layer would not exist when the flow velocity (U) was larger than $0.8U_{ca}$ and thus, the local scour process would be independent of the sand non-uniformity.

Fig.12 presents the temporal maximum scour depth at the upstream corners of the pile of tests B2 and C. Similar to the case of test B2 (uniform sand bed), the maximum scour depth of test C increased rapidly in the initial stage and is a constant value in the equilibrium stage. Each scour duration of tests B2 and C for the equilibrium scour depth was approximately 14400 s. The sand non-uniformity of test B2 (σ=1.6) was only 0.34 larger than test C (σ=1.26); thus, the former equilibrium scour depth (7.6 cm) was approximately 55% larger than the latter one (4.9 cm). The substantially large scour hole size, extensive bed profile, nearly equaled equilibrium scour duration, and deep scour depth indicated that the sediment transport rate of test C in uniform sand conditions was considerably more efficient than test B2 in non-uniform sand conditions.

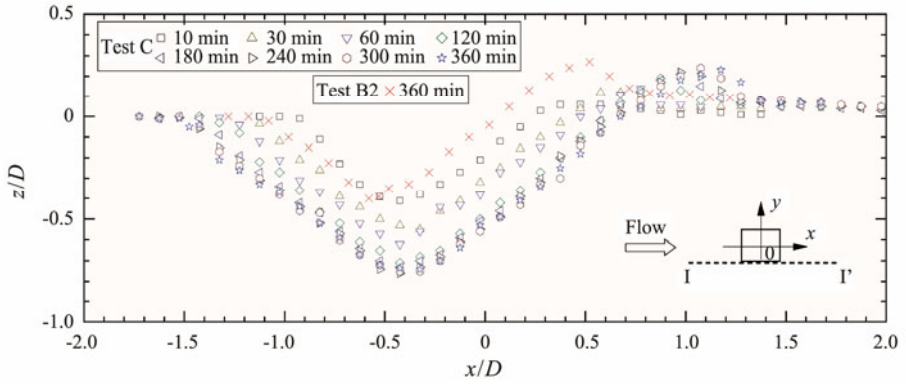

Fig.11 Bed elevations of test B2 at 360 min and temporal bed elevations of test C.

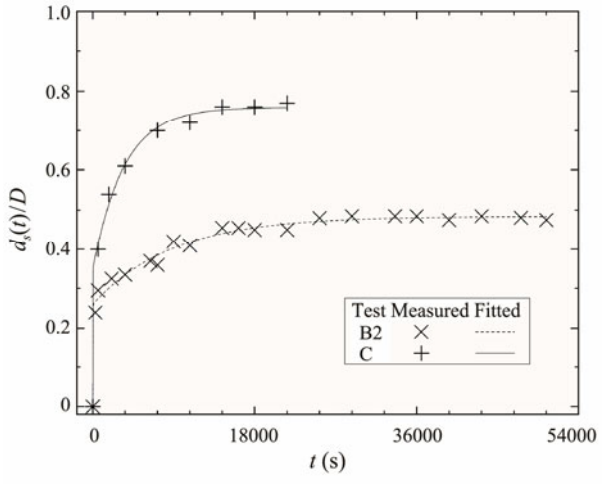

Fig.12 Temporal maximum scour depth of tests B2 and C fitted with Eq. (4).

6 Conclusions

The influences of flow depth on local scour around a submerged square pile were experimentally studied in uniform and non-uniform sand in a steady flow. Evolution characteristics of bed profiles, temporal maximum scour depth, and sand scour and deposition were analyzed. Relationships between the equilibrium scour depth and flow depth were quantified. The main conclusions can be summarized as follows.

In uniform sand beds, the characteristics of bed profiles and the history of the maximum scour depth varied minimally with the increasing flow depth. Scour depth at the stagnation point ranged from 0 to 0.03D, which was far less than that at the upstream corners, illustrating the horse-shoe vortex played a minor role in local scour when the flow intensity was insufficiently high. The temporal maximum scour depth data were fitted very well with Eqs. (2) and (3). The relative equilibrium scour depth was independent of the relative flow depth when the latter was larger than 1.5. This value nearly equaled that in an unsubmerged case of a circular pile given in the literature.

In a non-uniform sand bed, the equilibrium scour depth was reduced by more than 50% due to the armoring effects of coarse sediment particles on fine particles. Eq. (4) was substantially better in predicting the history of the maximum scour depth than Eqs. (2) and (3) because the developing stage duration was considerably longer in a

high flow intensity in clear-water scour conditions. Scour depth at the upstream corners was approximately one time larger than that at the stagnation point for each test. These differences from the low flow intensity conditions in uniform beds indicated that the effect of flow intensity was more important than the flow depth in determining the horseshoe vortex strength. The relative equilibrium scour depth was independent of the relative flow depth or submergence ratio when the latter was larger than 3 or 2, respectively.

The sediment scours and deposition patterns, as well as the bed profiles, were similar to each other in uniform and non-uniform sand bed conditions. The evolutions of bed profiles varied correspondingly to the temporal maximum scour depth in each test. The paralleled scour hole slopes and the scour hole depth that represented the size of a scour hole were governed by the combinations of the angle of sediment repose and the flow accelerations upstream of the pile.

Acknowledgements

The authors acknowledge the support of the National Natural Science Foundation of China (Nos. 51679223 and 51739010), the 111 Project (No. B14028), the Shangdong Provincial Key Laboratory of Ocean Engineering (No. kl oe202009), the Ningbo Natural Science Foundation (No. 2021J096), and a grant from the 7th Generation Ultra-Deepwater Drilling Rig Innovation Project.

References

Alejandra, C. O., Brina, M. M., and Mohammed, A. G., 2021. Bridge pier scour: An overview of factors affecting the phenomenon and comparative evaluation of selected models. *Transportation Geotechnics*, **28**: 100549, https://doi.org/10.1016/j.trgeo.2021.100549.

Baker, C. J., 1979. The laminar horseshoe vortex. *Journal of Fluid Mechanics*, **95** (2): 344-367, https://doi.org/10.1017/S0022112079001506.

Bordbar, A., Sharifi, S., and Hemida, H., 2021. Investigation of the flow behaviour and local scour around single square-shaped cylinders at different positions in live-bed. *Ocean Engineering*, **238**: 109772, https://doi.org/10.1016/j.oceaneng.2021.109772.

Briaud, J. L., Ting, F. C. K., Cheng, H. C., Gudavalli, R., Perugu, S., and Wei, G. S., 1999. SRICOS: Prediction of scour rate in cohesive soils at bridge piers. *Journal of Geotechnical and Environmental Engineering*, **125** (4): 237-246, https://doi.org/10.1061/(ASCE)1090-0241(2000)126:11(1028).

Cheng, N., and Zhao, K., 2017. Difference between static and dynamic angle of repose of uniform sediment grains. *International Journal of Sediment Research*, **32** (2): 149-154, https://doi.org/10.1016/j.ijsrc.2016.09.001.

Dey, S., Raikar, R. V., and Roy, A., 2008. Scour at submerged cylindrical obstacles under steady flow. *Journal of Hydraulic Engineering*, **134** (1): 105-109, https://doi.org/10.1061/(ASCE)0733-9429(2008)134:1(105).

Du, S., and Liang, B., 2019. Comparisons of local scouring for submerged square and circular cross-section piles in steady currents. *Water*, **11**: 1820, https://doi.org/10.3390/w11091820.

Du, S., Wang, Z., Wang, R., Liang, B., and Pang, X., 2022. Effects of flow intensity on local scour around a submerged square pile in steady current. *Physics of Fluids*, **34**: 085126, https://doi.org/10.1063/5.0103556.

Ettema, R., Constantinescu, G., and Melville, B. W., 2017. Flow-field complexity and design estimation of pier-scour depth: Sixty years since laursen and toch. *Journal of Hydraulic Engineering*, **143** (9): 03117006, https://doi.org/10.1061/(ASCE)HY.1943-7900.0001330.

Euler, T., and Herget, J., 2011. Obstacle-Reynolds-number based analysis of local scour at submerged cylinders. *Journal of Hydraulic Research*, **49** (2): 267-271, https://doi.org/10.1080/00221686.2010.547719.

Gao, J., Ma, X., Dong, G., Chen, H., Liu, Q., and Zang, J., 2021. Investigation on the effects of Bragg reflection on harbor oscillations. *Coastal Engineering*, **170**: 103977, https://doi.org/10.1016/j.coastaleng.2021.103977.

Gao, J., Ma, X., Zang, J., Dong, G., Ma, X., Zhu, Y., *et al*., 2020. Numerical investigation of harbor oscillations induced by focused transient wave groups. *Coastal Engineering*, **158**: 103670.

Guan, D., Chiew, Y. M., Wei, M., and Hsieh, S. C., 2019. Characterization of horseshoe vortex in a developing scour hole at a cylindrical bridge pier. *International Journal of Sediment Research*, **34** (2): 118-124, https://doi.org/10.1016/j.ijsrc.2018.07.001.

Hunt, D., 2009. Monitoring scour critical bridges. NCHRP synthesis 396. Transportation Research Board, Washington, D. C., https://doi.org/10.17226/22979.

Khosronejad, A., Kang, S., and Sotiropoulos, F., 2012. Experimental and computational investigation of local scour around bridge piers. *Advances in Water Resources*, **37**: 73-85, https://doi.org/10.1016/j.advwatres.2011.09.013.

Lacey, R. W. J., and Rennie, C. D., 2012. Laboratory investigation of turbulent flow structure around a bed-mounted cube at multiple flow stages. *Journal of Hydraulic Engineering*, **138** (1): 71-84, https://doi.org/10.1061/(asce)hy.1943-7900.0000476.

Liang, B., Du, S., Pan, X., and Zhang, L., 2020. Local scour for vertical piles in steady currents: Review of mechanisms, influencing factors and empirical equations. *Journal of Marine Science and Engineering*, **8** (1): 4, https://doi.org/10.3390/jmse8010004.

Liu, K., Liu, J. L., and Yu, W. C., 2019. Statistical analysis of bridges caused by floods from 2007 to 2015. *Urban Roads Bridges Flood Control*, **1**: 90-92, https://doi.org/10.16799/j.cnki.csdqyfh.2017.01.025 (in Chinese with English abstract).

Melville, B. W., 1997. Pier and abutment scour−An integrated approach. *Journal of Hydraulic Engineering*, **123** (2): 125-136, https://doi.org/10.1061/(ASCE)0733-9429(1997)123:2(125).

Melville, B. W., and Chiew, Y. M., 1999. Time scale for local scour at bridge piers. *Journal of Hydraulic Engineering*, **125** (1): 59-65, https://doi.org/10.1061/(ASCE)0733-9429(1999)125:1(59).

Melville, B. W., and Sutherland, A. J., 1988. Design method for local scour at bridge piers. *Journal of Hydraulic Engineering*, **114** (10): 1210-1226, https://doi.org/10.1061/(ASCE)0733-9429(1988)114:10(1210).

Mir, B. H., Lone, M. A., Bhat, J. A., and Rather, N. A., 2018. Effect of gradation of bed material on local scour depth. *Geotechnical and Geological Engineering*, **36** (4): 2505-2516, https://doi.org/10.1007/s10706-018-0479-x.

Okamoto, S., and Sunabashiri, Y., 1992. Vortex shedding from a circular cylinder of finite length placed on a ground plane. *Transactions ASME, Journal of Fluids Engineering*, **114**: 512-521, https://doi.org/10.1115/1.2910062.

Oliveto, G., and Hager, W. H., 2002. Temporal evolution of clear-water pier and abutment scour. *Journal of Hydraulic Engineering*, **128** (9): 811-820, https://doi.org/10.1061/(ASCE)07

33-9429(2002)128:9(811).

OuYang, H., Dai, G., Gao, L., Zhu, W., Du, S., and Gong, W., 2022. Local scour characteristics of monopile foundation and scour protection of cement-improved soil in marine environment–Laboratory and site investigation. *Ocean Engineering*, **255**: 111443, https://doi.org/10.1016/j.oceaneng.2022.111443.

Roulund, A., Sumer, B. M., Fredsøe, J., and Michelsen, J., 2005. Numerical and experimental investigation of flow and scour around a circular pile. *Journal of Fluid Mechanics*, **534** (534): 351-401, https://doi.org/10.1017/S0022112005004507.

Rudolph, D., Raaijmakers, T., and Stam, C., 2008. Time-dependent scour development under combined current and wave conditions–Hindcast of field measurements. *Proceedings 4th Internation Conference on Scour Erosion (ICSE*). Tokyo, 340-347, https://henry.baw.de/handle/20.500.11970/100109.

Sarkar, A., 2014. Scour and flow around submerged structures. *Proceedings of the ICE-Water Management*, **167** (2): 65-78, https://doi.org/10.1680/wama.12.00117.

Shamloo, H., Rajaratnam, N., and Katopodis, C., 2001. Hydraulics of simple habitat structures. *Journal of Hydraulic Research*, **39** (4): 351-366, https://doi.org/10.1080/00221680109499840.

Sheppard, D. M., Odeh, M., and Glasser, T., 2004. Large scale clear-water local pier scour experiments. *Journal of Hydraulic Engineering*, **130** (10): 957-963, https://doi.org/10.1061/(ASCE)0733-9429(2004)130:10(957).

Simarro, G., Teixeira, L., and Cardoso, A. H., 2007. Flow intensity parameter in pier scour experiments. *Journal of Hydraulic Engineering*, **133** (11): 1261-1264, https://doi.org/10.1061/(ASCE)0733-9429(2007)133:11(1261).

Sumer, B. M., and Fredsøe, J., 2002. The mechanics of scour in the marine environment. *Advanced Series on Ocean Engineering*, **17**: 552, https://doi.org/10.1142/4942.

Tseng, M. H., Yen, C. L., and Song, C. C. S., 2000. Computation of three-dimensional flow around square and circular piers. *International Journal for Numerical Methods in Fluids*, **34** (3): 207-227, https://doi.org/10.1002/1097-0363(20001015)34:3<207::AID-FLD31>3.0.CO;2-R.

Tsutsui, T., 2012. Flow around a cylindrical structure mounted in a plane turbulent boundary layer. *Journal of Wind Engineering and Industrial Aerodynamics*, **104-106**: 239-247, https://doi.org/10.1016/j.jweia.2012.05.003.

Wang, C., Huang, B., Xu, T., David, Z. Z., Wang, L., and Wang, Y., 2022. Numerical modeling of energy dissipation of internal solitary waves encountering step topography. *Ocean Engineering*, **259**: 111853, https://doi.org/10.1016/j.oceaneng.2022.111853.

Williams, P., Balachandar, R., Roussinova, V., and Barron, R., 2022. Particle image velocimetry evaluation of flow-altering countermeasures for local scour around a submerged circular cylinder. *International Journal of Sediment Research*, **37** (4): 411-423, https://doi.org/10.1016/j.ijsrc.2022.03.001.

Yang, F., Qu, L., Zhang, Q., Tang, G., and Liang, B., 2021. Local scour around tandem square porous piles in steady current. *Ocean Engineering*, **236**: 109554, https://doi.org/10.1016/j.oceaneng.2021.109554.

Yao, W. D., An, H. W., Draper, S., Cheng, L., and Harris, J. M., 2018. Experimental investigation of local scour around submerged piles in steady current. *Coastal Engineering*, **142**: 27-41, https://doi.org/10.1016/j.coastaleng.2018.08.015.

Zhang, Q., Tang, G., Lu, L., and Yang, F., 2021. Scour protections of collar around a monopile foundation in steady current. *Applied Ocean Research*, **112**: 102718, https://doi.org/10.1016/j.apor.2021.102718.

Zhao, M., Cheng, L., and Zang, Z., 2010. Experimental and numerical investigation of local scour around a submerged vertical circular cylinder in steady currents. *Coastal Engineering*, **57** (8): 709-721, https://doi.org/10.1016/j.coastaleng.2010.03.002.

Zhao, M., Zhu, X., Cheng, L., and Teng, B., 2012. Experimental study of local scour around subsea caissons in steady currents. *Coastal Engineering*, **60** (1): 30-40, https://doi.org/10.1016/j.coastaleng.2011.08.004.

(Edited by Chen Wenwen)